Influence of heterogeneous thermal conductivity on the long-term evolution of the lower mantle thermochemical structure: implications for primordial reservoirs

Joshua M. Guerrero[1], Frédéric Deschamps[1], Yang Li[2], Wen-Pin Hsieh[1], and Paul J. Tackley[3]

[1]Institute of Earth Sciences, Academia Sinica, Taipei
[2]State Key Laboratory of Lithospheric Evolution, Institute of Geology and Geophysics, Institutions of Earth Science, Chinese Academy of Sciences, Beijing
[3]Department of Earth Sciences, ETH Zürich, Zürich

Correspondence: Joshua Martin Guerrero (joshua@earth.sinica.edu.tw), Frédéric Deschamps (frederic@earth.sinica.edu.tw)

Abstract. The long-term evolution of the mantle is simulated using 2D spherical annulus geometry to examine the effect of heterogeneous thermal conductivity on the stability of reservoirs of primordial material. In numerical models, mantle conductivity is often emulated using purely depth-dependent profiles (taking on values between 3 and 9 $\mathrm{Wm^{-1}K^{-1}}$). This approach is meant to synthesize the mean conductivities of mantle materials at their respective conditions in-situ. However, because conductivity depends also on temperature and composition, the effects of these dependencies in mantle conductivity is masked. This issue is significant because dynamically evolving temperature and composition introduce lateral variations in conductivity, especially in the deep-mantle. Minimum and maximum variations in conductivity are due to the temperatures of plumes and slabs, respectively, and depth-dependence directly controls the amplitude of the conductivity (and its variations) across the mantle depth. Our simulations allow assessing the consequences of these variations on mantle dynamics, in combination with the reduction of thermochemical pile conductivity with iron composition, which has so far not been well examined. We find that the temperature- and depth- variations combined characterize the mean conductivity ratio from top-to-bottom. For the mean conductivity profile to be comparable to the conductivity often assumed in numerical models, the depth- dependent ratio must be at least 9 times the surface conductivity. When the conductivity profile is underestimated, the imparted thermal buoyancy (from heat-producing element (HPE) enrichment) destabilizes the reservoirs and influences core-mantle boundary (CMB) coverage configuration and the onset of entrainment. The compositional correction for conductivity only plays a minor role that behaves similarly to conductivity reduction due to temperature. Nevertheless, this effect may be amplified when depth-dependence is increased. For the cases we examine, when the lowermost mantle's mean conductivity is greater than the surface conductivity, reservoirs can remain stable for periods exceeding the age of the solar system.

1 Introduction

Tomographic studies of Earth's lower mantle revealed the presence of two large low velocity provinces (LLVPs) that overlie the core-mantle boundary (CMB). They are located below the Pacific ocean and Africa with a combined coverage of up to 30% of the CMB and vertical extents as high as 1200 km (Garnero et al., 2016). These anomalous regions have been characterized

by either purely thermal (Davies et al., 2012) or combined thermal and chemical (e.g., Trampert et al., 2004) effects (the latter case being aptly referred to as thermochemical piles). Piles may further affect plume generation (e.g., Tan et al., 2011; Heyn et al., 2020) and core-to-mantle heat flow (e.g., Deschamps & Hsieh, 2019). Furthermore, plumes sourced from deep mantle reservoirs may provide a mechanism to explain the diverse chemistry observed in ocean island basalts (Deschamps et al., 2011). In light of this fact, while there are two end-member views on their origin (and chemical composition), a primordial layer (composed of anomalously dense material) or a growing layer (composed of mid-ocean ridge basalt), in this study we adopt the former.

Piles' unique chemical composition determines physical properties such as density, viscosity, thermal conductivity, and enrichment in HPEs that affect their long-term stability (e.g., Li et al., 2014, 2018, 2019; Gülcher et al., 2020; Citron et a., 2020). In numerical simulations, underestimating their density and viscosity contrasts with respect to the ambient mantle can result in overestimating the entrainment of dense material. In these studies, radially defined conductivity profiles synthesized and emulated the mean contributions from either (or all of) temperature, pressure (and hence, depth), and chemical composition. Until very recently, the effect of thermal conductivity had not been well examined in simulations featuring a compressible fluid and thermochemical piles. Li et al. (2022) showed that compositional corrections to conductivity can raise the topography of thermochemical piles.

Temperature and depth variations in conductivity had been considered previously for Boussinesq or extended Boussinesq fluid simulations. Utilizing Hofmeister (1999)'s lattice conductivity formulation in an isoviscous Boussinesq fluid, several effects were observed: temperature increases in the lower mantle (Dubuffet et al., 1999), a stabilizing effect on mantle flow, which manifests in thick and stable plumes (Dubuffet & Yuen, 2000), and the rapid thermal assimilation of cold downwelling slabs (Dubuffet et al., 2000). Yanagawa et al. (2005) examined the effects of a purely temperature dependent conductivity in conjunction with a strongly temperature dependent viscosity and observed a cooler, thinner, upper thermal boundary layer when compared to a constant conductivity. More recently, Tosi et al. (2013) parametrized a temperature and pressure dependent thermal conductivity (and thermal expansivity) derived from mineral physics data. They observed a strong increase in bulk mantle temperature, which suppresses bottom thermal boundary layer instabilities and causes mantle flow to be driven by instabilities at the upper thermal boundary.

In this study, we examine the effect of temperature-, depth-, and compositional- dependent conductivity on the stability of thermochemical piles.

2 Methods

2.1 General physical properties

We model compressible thermochemical mantle convection using the finite volume code StagYY (Tackley, 2008). Each calculation is performed in a 2D spherical annulus domain, which emulates convection in a variable-thickness slice of a spherical shell centred at the equator (Hernlund & Tackley, 2008). The reference state characterizing compressible convection is based on the calculations presented in Tackley (1998). The parameters defining this reference state are listed in the Table S1 and

illustrated in Figure S1 of the Supplement. We model a phase change between upper and lower mantle materials but neglect the phase change from perovskite to post-perovskite at the bottom of the mantle. Thermochemical reservoirs are modelled with a dense primordial material origin. An initial dense layer occupies the bottom 160 km of the lower mantle, corresponding to a volume fraction of approximately 3%. The buoyancy ratio, B, defines the density contrast between regular and primordial

60   materials. We prescribe a value of 0.23, which corresponds to a density contrast of 95 $\mathrm{kgm^{-3}}$ near the surface and 152 $\mathrm{kgm^{-3}}$ near the CMB. The mantle is basally heated and is also internally heated by heat-producing elements (HPEs) and we prescribe a non-dimensional heating rate, $H = 20$, which corresponds to a dimensional heating rate of 5.44×10^{-12} $\mathrm{Wkg^{-1}}$. We assume primordial material is enriched in HPEs and has a rate up to an order of magnitude greater than regular mantle material. The initial temperature field is based on an adiabatic temperature profile of 2000 K with surface and core-mantle boundary layer

65   thicknesses of approximately 30 km. Random temperature perturbations with an amplitude of 125 K are uniformly distributed throughout the domain. The surface and core-mantle boundary temperatures are defined at 300 K and 3440 K, respectively. Mantle viscosity featuring depth-, temperature-, and composition- dependence is modelled using an Arrhenius formulation. A yield stress of 290 MPa is imposed at the surface so that the development of a stagnant-lid is avoided. Viscosity is truncated so that nondimensional viscosity values do not exceed 10^5 or fall below 10^{-3} of the reference viscosity.

70   ## 2.2   Thermal conductivity

Heterogeneous conductivity is emulated using a non-dimensional parametrized model that characterizes variations resulting from non-dimensional depth, $\tilde{d} = d/D$, where the depth, d, has length scale defined by the mantle thickness, D; non-dimensional temperature, $\tilde{T} = T/\Delta T_S$, where the temperature, T, is scaled by the super-adiabatic temperature difference, ΔT_S; and composition, C; as separate functions. Thermal conductivity is non-dimensionalized with its surface value k_S,

75   which is here fixed to 3 $\mathrm{Wm^{-1}K^{-1}}$. The total conductivity is a product of each individual functional dependence. In this study, we first consider a linear depth- dependence given by

$$\tilde{k}_D(\tilde{d}) = 1 + (K_D - 1)\tilde{d} \tag{1}$$

to explicitly examine the effect of top-to-bottom conductivity ratio. This conductivity ratio is controlled by the parameter, K_D, so that the non-dimensional depth- dependent conductivity takes on values between 1 and K_D.

80   Next, we consider depth- dependence based on conductivity measurements of minerals in the upper and lower mantles. Conductivity values in the lower mantle were based on a parametrization of conductivity profiles (defined in Deschamps & Hsieh (2019)) for a 20%-bridgmanite (Bm) and 80%-ferropericlase (Fp) mixture. Measurements for bridgmanite were presented by Hsieh et al. (2017) and for ferropericlase by Hsieh et al. (2018). The conductivity profile in the upper mantle is defined by a quadratic that smoothly connects the surface conductivity to the conductivity profile of Bm-Fp at the 660-km

85   transition. We find that there is good agreement between the modelled conductivity profile and the measurements of dry and wet olivine presented by Chang et al. (2017). The total conductivity profile is defined piecewise and continuous at the 660-km

transition ($\tilde{d}_{ULM} = 0.22837$) and is given by

$$\tilde{k}_D(\tilde{d}) = \begin{cases} \frac{3.0}{k_S}\left(1 + 15.66\tilde{d} - 16.38\tilde{d}^2\right); & \tilde{d} < \tilde{d}_{ULM} \quad \text{(Upper mantle)} \\ \frac{5.33}{k_S}\left(1 + 4.98\tilde{d} - 0.81\tilde{d}^2\right); & \tilde{d} \geq \tilde{d}_{ULM} \quad \text{(Lower mantle)} \end{cases} \tag{2}$$

The top-to-bottom conductivity ratio is 9.185 and this depth- dependence is referred to as $K_D = 9.185$ in this study. Compared
90 with the linear $K_D = 10$ depth- profile, the quadratic depth- dependence is slightly raised near the transition zone and slightly
lowered near the CMB. Depth- dependent conductivity profiles are illustrated in Figure 1.
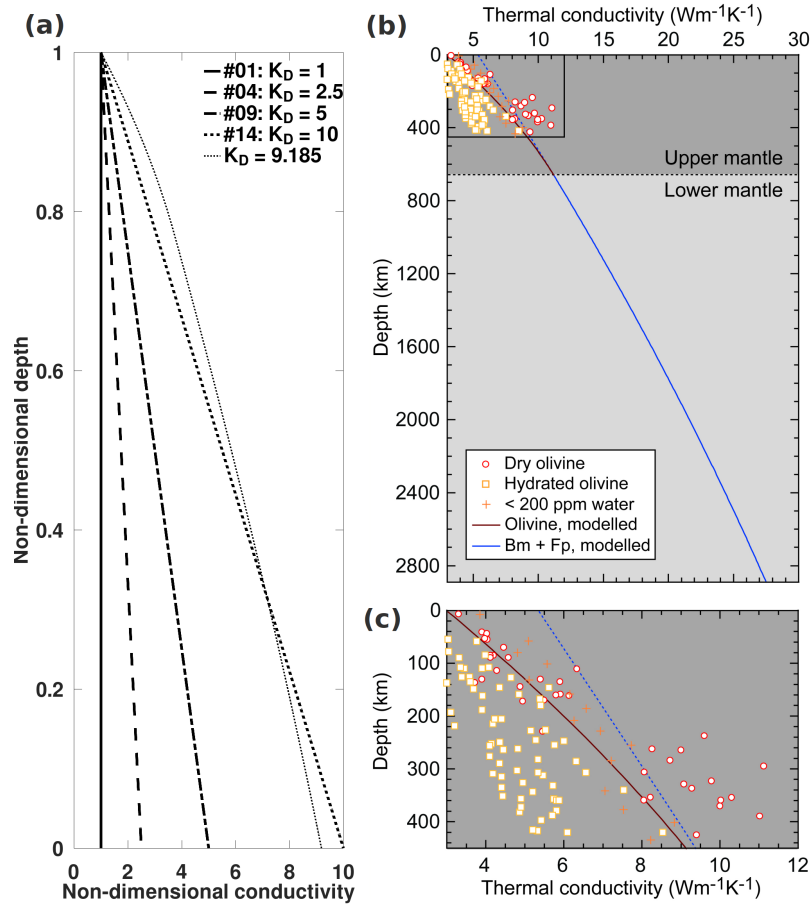
Figure 1. (a) Radial profiles for different depth- dependent conductivity functions characterized by different K_D values. (b) Conductivity
measurements for upper and lower mantle materials. Olivine data points are from Chang et al. (2017) and the modelled Bm+Fp conductivity
profile is based on data presented in Hsieh et al. (2017) and Hsieh et al. (2018). (c) Magnification of conductivity profile in the upper mantle.

Temperature- dependence is given by

$$\tilde{k}_T(\tilde{T}) = \left(\frac{(T_{surf}/\Delta T_S)}{\tilde{T}}\right)^n, \tag{3}$$

which always results in lower thermal conductivity. The super-adiabatic temperature difference, ΔT_S, is set to 2500 K. Higher

95 values of n indicate higher sensitivity to (and greater reduction with) increasing temperature. In this study, we consider n values

of 0.5 and 0.8. The theoretical lower limit for n is 0.5, for materials that are enriched in iron, and a value of 0.8 is representative

of oxides (e.g., Klemens, 1960; Xu et al., 2004). When n is 0.0, temperature- dependence is neglected and only the remaining

dependences are considered.

Composition- dependence is given by

100 $\tilde{k}_C(C) = 1 + (K_C - 1)C$ (4)

where K_C is the factor for compositional correction. For the primordial material considered in this study we consider cor-

rections of 0.8 and 0.5 (corresponding to 20% and 50% conductivity reduction, respectively). When K_C is 1.0, compositional

correction is neglected. Finally, the total conductivity is given by

$k(d, T, C) = k_S \times \tilde{k}_D(d) \times \tilde{k}_T(T) \times \tilde{k}_C(C).$ (5)

105 Simulations are computed over a non-dimensional diffusion time of 0.0318, corresponding to 11.2 Gyr in dimensional units.

Note that because they do not include mantle initial conditions, which are not known, and time-decreasing radioactive heating,

our simulations are not meant to model the mantle evolution, and duration should not be used to interpret specific sequences

of events. The longer simulation time is necessary to allow the simulations' heat flows to achieve a quasi-steady state. Using

this setup, we run 19 simulations exploring the impact of conductivity variations (Table 1). All observable and derived physical

110 properties are averaged over a 2 Gyr window centred about $t = 4.5$ Gyr (illustrated in Figure 2) and are presented in Table 1.

Complete details of the methods are included in the Supplement.

3 Results

To measure the evolution of the thermochemical structure, we examined quasi-stationary periods determined by the systems'

mean heat flows. The stability of thermochemical reservoirs was assessed by their mean temperature, T_{prim}; average height,

115 h_C; and coverage of the CMB, A_{CMB} (Figure 2). The onset of instability, $t_{inst.}$, is calculated by examining time derivatives

of average heights of primordial material (see the Supplement for details).

3.1 Effect of heterogeneous conductivity featuring reference depth-dependence

We first defined a purely depth- dependent reference case characterized by depth- dependence, $K_D = 2.5$, with lower mantle

conductivities comparable to current estimates (e.g., Deschamps & Hsieh, 2019; Geballe et al., 2020). Heat flows for our mod-

120 els reached a quasi-steady state by approximately 4 Gyr. We found that temperature- dependent conductivity greatly reduced

both CMB and surface heat flows (by approximately 75% and 20%, respectively), as less heat can be extracted from the base.

Furthermore, we find that compositional correction is of secondary importance, in agreement with Li et al. (2022) findings.

Despite a 20% reduction in the conductivity of primordial material (green), Q_{CMB} is marginally greater. Similarly, Q_{CMB} is
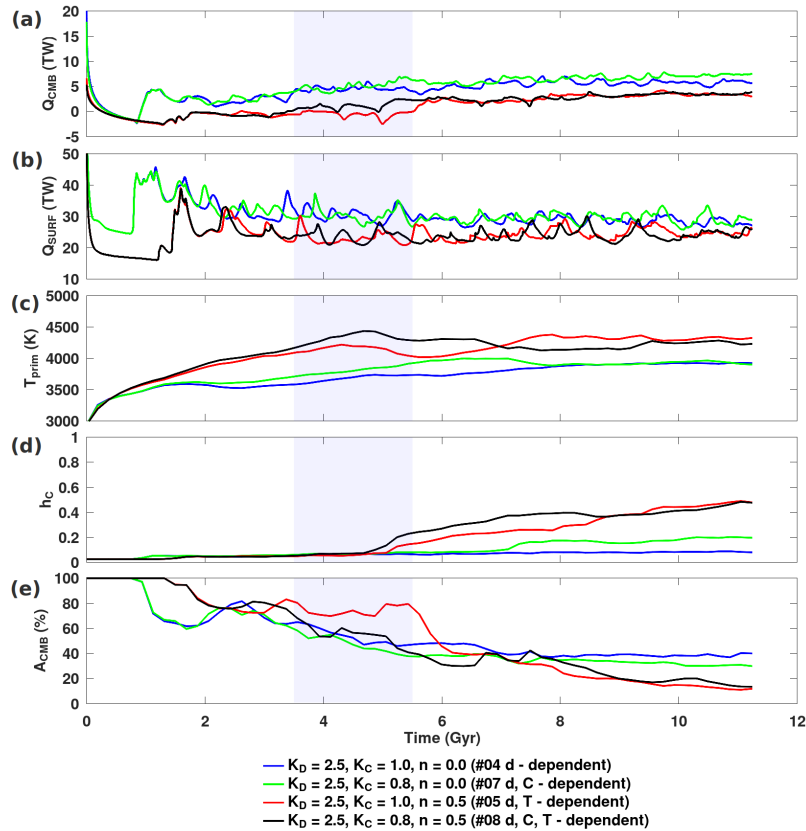
Figure 2. Evolution of cases featuring $K_D = 2.5$. The quasi-stationary period centred about 4.5 Gyr is shaded in gray.

greater when temperature- dependent conductivity included compositional correction. This behaviour is likely owing to less

125 CMB coverage in composition corrected cases. Differing conductivity conditions can result in many thermochemical reservoir evolution and cooling histories. For example, with long-standing CMB coverage (red curve), extended periods of mean negative heat flux were possible, and positive heat flux occurs once the piles become unstable and the CMB is liberated of primordial material. Determining the mechanisms that trigger these different outcomes will provide constraints for plausible mantle conductivity models.

130 For the cases presented, T_{prim} increased marginally due to compositional correction and increased significantly with temperature dependence. In general, T_{prim} increases when thermochemical reservoir conductivity is reduced. Only until h_C had increased (i.e., piles became unstable and started eroding) T_{prim} decreased. Temperature- dependence greatly amplifies T_{prim} and is the dominant effect over composition. The long-term evolution of reservoirs characterized by a marginal temperature increase may result in a stable arrangement of piles with increased topography with respect to the initial layering (see Figure

135 S2, #07), whereas, a substantial increase in temperature (i.e., exceeding approximately 500 K) may result in the entrainment

of piles (see Figure S2, #08). Between these two cases, the onset of instability differs by approximately 2 Gyr. Examining the differences in system's conductivity fields (profiles and top-to-bottom conductivity ratios) clarify these observations.

Table 1. Averaged properties for all cases presented. All values are computed within in a 2 Gyr period encompassing 4.5 Gyr.

Case #	K_D	K_C	n	T_{mean} (K)	T_{prim} (K)	global rms dT_{prim} (K)	negative rms dT_{prim} (K)	positive rms dT_{prim} (K)	$\Delta T_{prim,max}$ (K)	Q_{SURF} (TW)	Q_{CMB} (TW)	h_C	A_{CMB}(%)	$t_{inst.}$ (Gyr)
1	1	1	0	2150	3930	450	350	550	1400	27.6	0.6	0.06	68	5.8
2	1	1	0.5	2380	4640	770	780	770	1540	23.7	1.0	0.26	36	3.9
3	1	1	0.8	2510	4900	820	830	810	1780	21.8	0.6	0.32	36	4.1
4	2.5	1	0	2200	3680	280	220	330	770	30.9	4.6	0.06	54	9.2
5	2.5	1	0.5	2370	4150	610	510	720	1480	23.3	-0.6	0.07	74	5.2
6	2.5	1	0.8	2500	4700	770	750	790	1620	22.2	0.2	0.13	51	4.5
7	2.5	0.8	0	2200	3810	390	300	480	970	30.6	5.1	0.07	48	7.1
8	2.5	0.8	0.5	2380	4330	670	600	740	1530	24.1	1.1	0.10	55	4.9
9	5	1	0	2230	3530	150	130	170	400	32.8	9.1	0.07	46	>11.2
10	5	1	0.5	2400	4050	490	400	580	1230	25.2	2.3	0.07	47	6.0
11	5	1	0.8	2490	4380	680	640	710	1430	21.4	0.0	0.07	61	5.4
12	5	0.8	0.5	2400	4160	560	480	640	1330	24.5	2.4	0.07	47	5.6
13	5	0.5	0.5	2410	4210	620	530	730	1530	23.9	1.7	0.08	57	5.2
14	10	1	0	2290	3410	90	110	80	190	36.4	14.7	0.06	48	>11.2
15	10	1	0.5	2400	3710	260	210	320	730	26.8	3.5	0.06	58	>11.2
16	10	1	0.8	2490	3950	470	380	570	1200	21.6	0.3	0.05	68	8.2
17	9.185	0.8	0.5	2380	3700	270	220	330	780	26.5	3.6	0.06	59	11.1
18	9.185	0.8	0.8	2470	4190	530	480	580	1170	22.7	1.5	0.07	49	6.6
19	9.185	0.5	0.5	2380	3820	420	320	520	1110	25.6	3.0	0.06	64	8.8

3.2 Effect of temperature- and depth- dependent conductivity
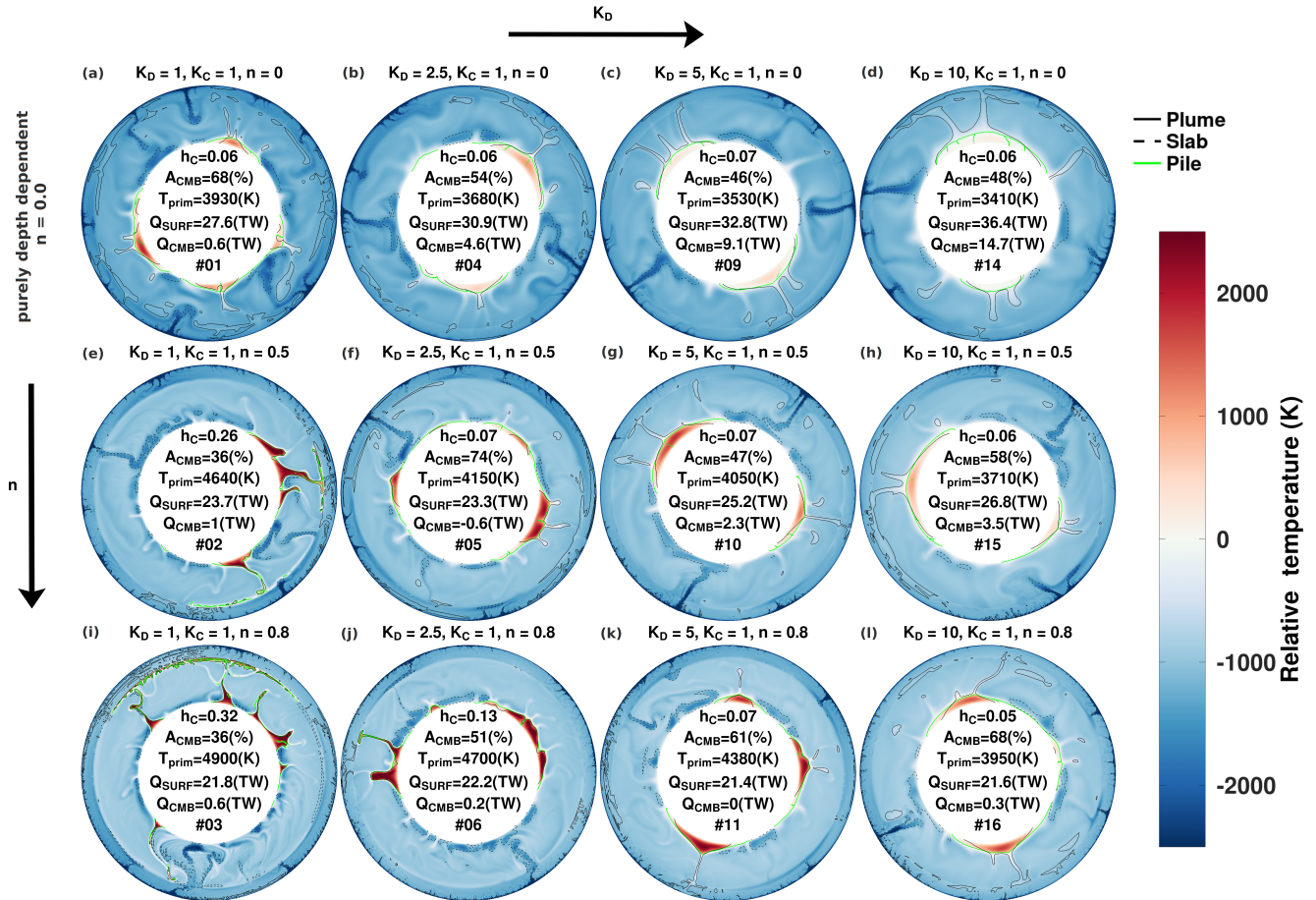
Figure 3. Temperature fields (relative to the CMB temperature) at 4.5 Gyr are shown for cases as a function of K_D and n. Averaged properties and case number are inset. (Primordial material fields are illustrated in Figure S3.)

First, we isolated the combined effect of temperature- and depth- dependent conductivities. Relative temperature fields are
140 presented in Figure 3 to illustrate the pile temperature excess with respect to the CMB temperature. Purely depth- dependent conductivity cases show that, a modest conductivity gradient ($K_D = 2.5$) was sufficient to stabilize the thermochemical reservoirs into a 2-pile configuration (by 4.5 Gyrs) (compare plots (a) and (b)). As K_D is further increased, reservoirs progress toward an antipodal arrangement. In addition, the increased conductivity in the lower mantle resulted in higher heat flows and cooler piles.

145 Figure 4 shows the thermal conductivity fields corresponding to cases presented in Figure 3. As n, and thus the temperature-dependence, was increased, a mean top-to-bottom conductivity ratio (≥ 1) may be established depending on K_D (e.g., Figure 4 plots (g) and (l), resulting in a 2-pile arrangement). When K_D is sufficient to produce a mean conductivity ratio ≥ 2, the hor-

izontally averaged conductivities near the CMB is much lower (~ 8 Wm^{-1}K^{-1} (#15)) compared to purely depth-dependent cases (30 Wm^{-1}K^{-1} (#14), for $K_D = 10$; Figure S4).

150   We observed that T_{prim} increased with greater temperature dependence (top-to-bottom rows in Figure 3). In addition, temperature still decreased with an increased depth-dependent gradient, K_D (e.g., Figure 4 plots (e) - (h), from ≤ 1 to > 1 mean conductivity ratio), but was not as reduced as in the purely depth- dependent cases. For cases with a mean conductivity ratio < 1, T_{prim} is in excess of 500 K of the T_{CMB} (e.g., (a),(e),(f),(i),(j), and (k)) resulting, again, in locally negative bottom heat flux within piles. The evolution of the reservoirs in these cases tends to eventual entrainment. The timing for the onset of insta-

155   bility, $t_{inst.}$, is listed for each case in Table 1. A pile's stability depends on how efficiently it can rid itself of heat. Therefore, the compositional correction to piles' conductivity must be examined in conjunction with the mantle's mean conductivity ratio.
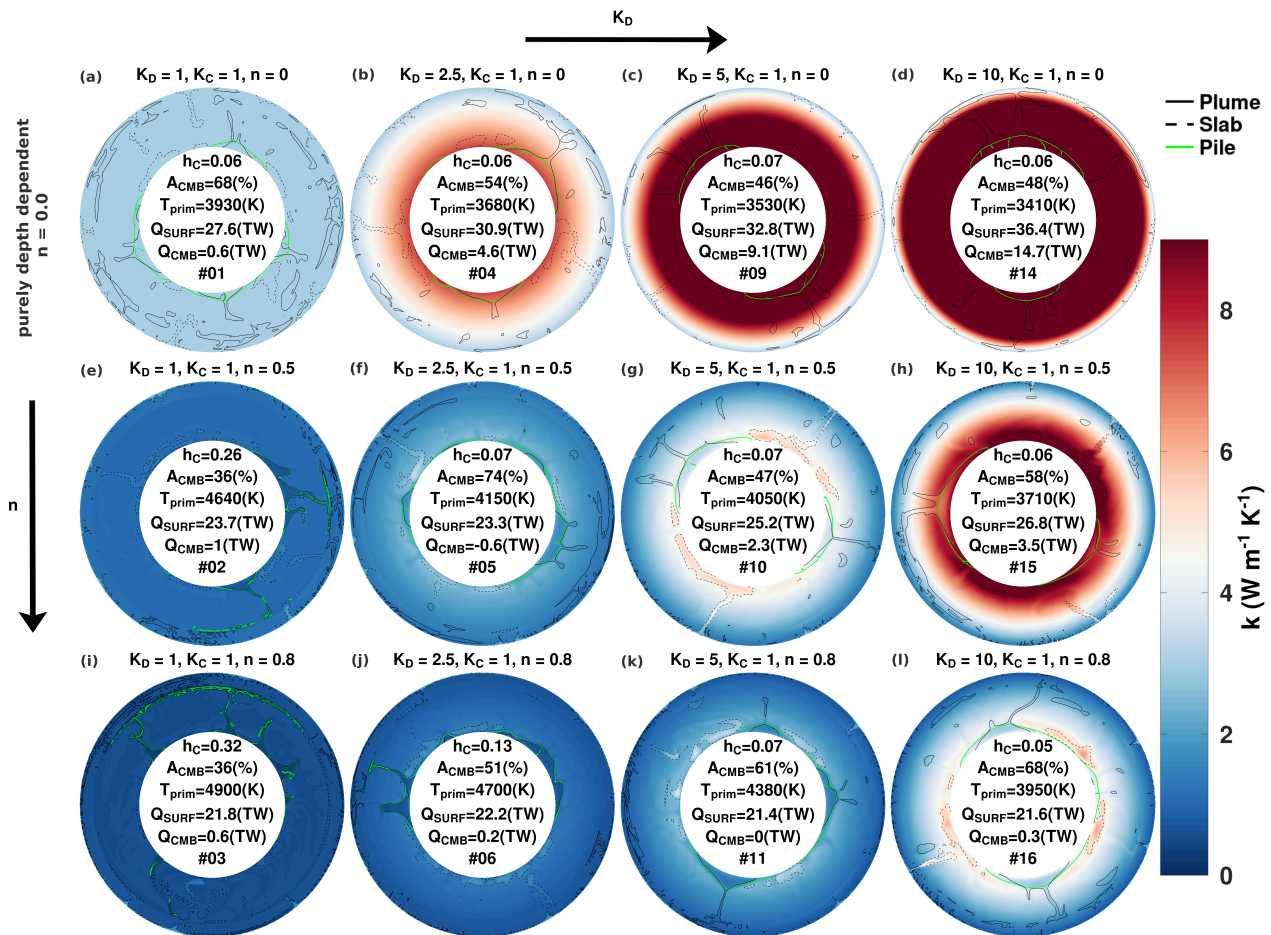
Figure 4. Conductivity fields corresponding to cases in Figure 3. The colour bar saturates at 9 Wm^{-1}K^{-1} so that the values in (c), (d), and (h) may be larger.

3.3 Including the effect of composition- dependent conductivity
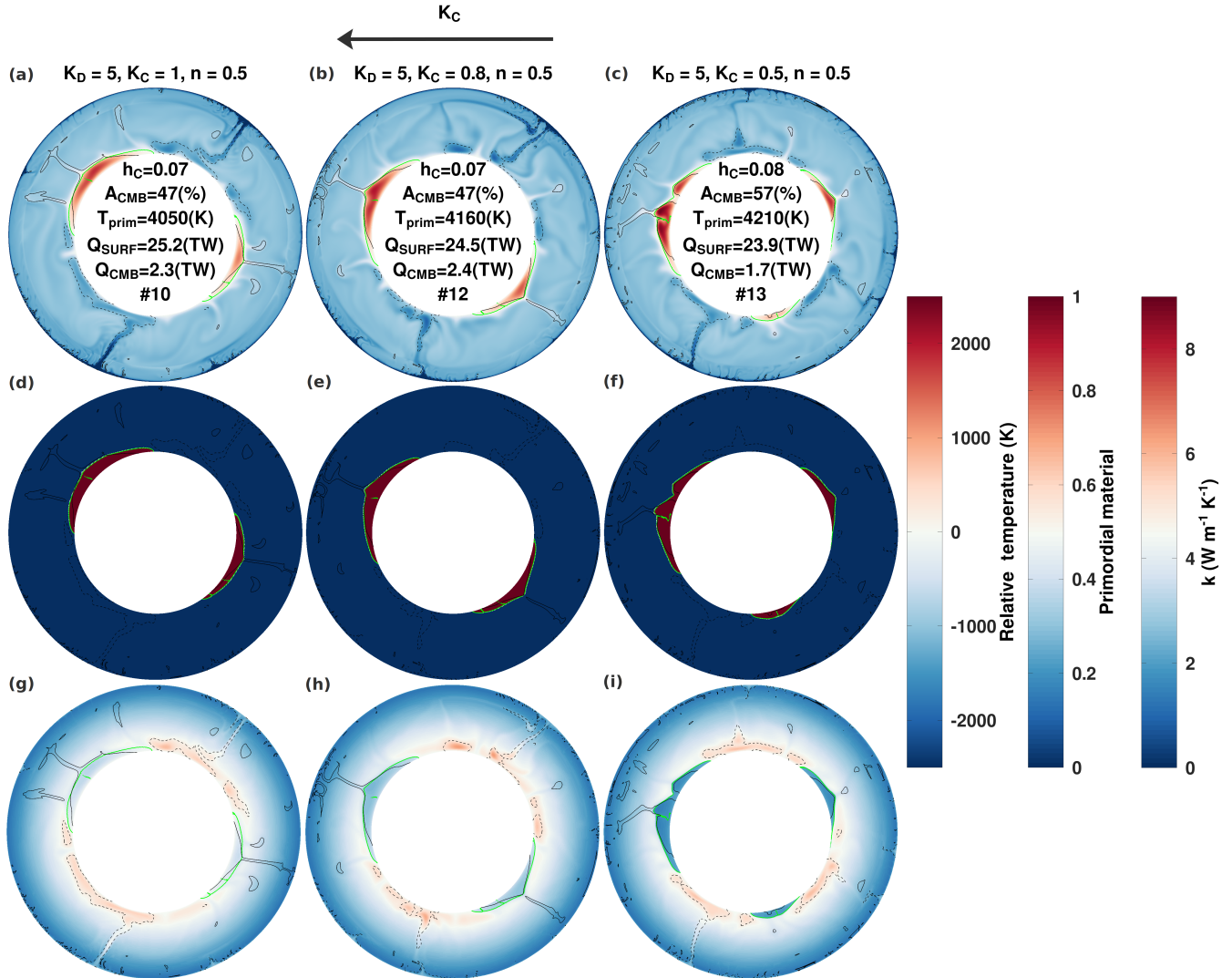
Figure 5. Temperature (relative to the CMB temperature) (top row), primordial material (middle row), and conductivity (bottom row) fields at 4.5 Gyr are shown for cases featuring decreasing K_C with $K_D = 5$ and $n = 0.5$. K_C is increases from right to left. Field values are indicated on the colour bars. Contours and inset values are defined similarly as in Figure 3.

The effect of compositional correction is highlighted for the case $K_D = 5$ and $n = 0.5$ (Figure 5). For this depth- dependence,
160 the mean lowermost mantle conductivity is greater than the surface conductivity and does not vary significantly when the conductivity of primordial material is reduced (i.e., less than $1\ \mathrm{Wm^{-1}K^{-1}}$ in the lowermost mantle; Figure S5). The maximum conductivity, characterized by the remnant downwelling material localized within the bottom 300 km, is approximately 2

$\mathrm{Wm^{-1}K^{-1}}$ higher than the mean conductivity profile. The minimum conductivity, characterized by the hottest regions of the reservoirs, is approximately $2\,\mathrm{Wm^{-1}K^{-1}}$ lower than the mean, and is localized near the tops of the piles, where the hottest

165   and most buoyant primordial material accumulates (approximately $500 - 800$ km above the CMB).

Pile temperature marginally increased when K_C was reduced. The additional thermal buoyancy imparted into the piles quickened the onset of instability. For this K_D value, the erosion of piles is initiated approximately 0.4 Gyr and 0.8 Gyr earlier from 6 Gyr when $K_C = 0.8$ and $K_C = 0.5$, respectively. Furthermore, pile configuration may change. When $K_C < 1$, single pile configuration can be attained as early as 8 Gyr (Figure S6).

170   ### 3.4   Long-term stability of thermochemical reservoirs featuring mineral physics derived conductivities

We now examine departures from moderate temperature- dependences ($n = 0.5$) and compositional corrections ($K_C = 0.8$) in conjunction with a depth- dependent profile derived from mineral conductivity measurements (Figure 6) and is equivalent to $K_D = 9.185$ (#17). In this case, thermochemical convection exhibits a stable 2-pile configuration during the entire simulation. When only K_C is reduced, from 0.8 to 0.5 (#19), the 2-pile configuration is also maintained throughout the simulation, but

175   episodes of bulk erosion in thin plume conduits are possible e.g., around 9 Gyr. Interestingly, the radial conductivity profile obtained by models #17 and #19 lead to average CMB conductivity close to the values estimated from mineral physics (Hsieh et al., 2018; Deschamps & Hsieh, 2019; Geballe et al., 2020). When only n is increased from 0.5 to 0.8 (#18), the onset of instability occurs approximately 5 Gyr sooner. The largest reservoir rapidly ejects dense material and by 11 Gyr the piles coalesce.

180   The distribution of light material ($C < 0.02$) is scattered about the lower mantle and may be ejected in small amounts into the upper mantle. An initial negative density anomaly is established compared with the mean mantle density (which is dominated by cold downwelling structures). When the thermochemical reservoirs finally become unstable, material with C between 0.02 and 0.90 is rapidly lifted away from the piles. This material dominates the mean density profile and produces a positive anomaly. The onset of light erosion precedes the onset of instability and the period between light and heavy erosion is

185   reduced when the mean conductivity gradient is reduced (e.g., dotted and dot-dashed curves in Figure 6, and Figure S7).
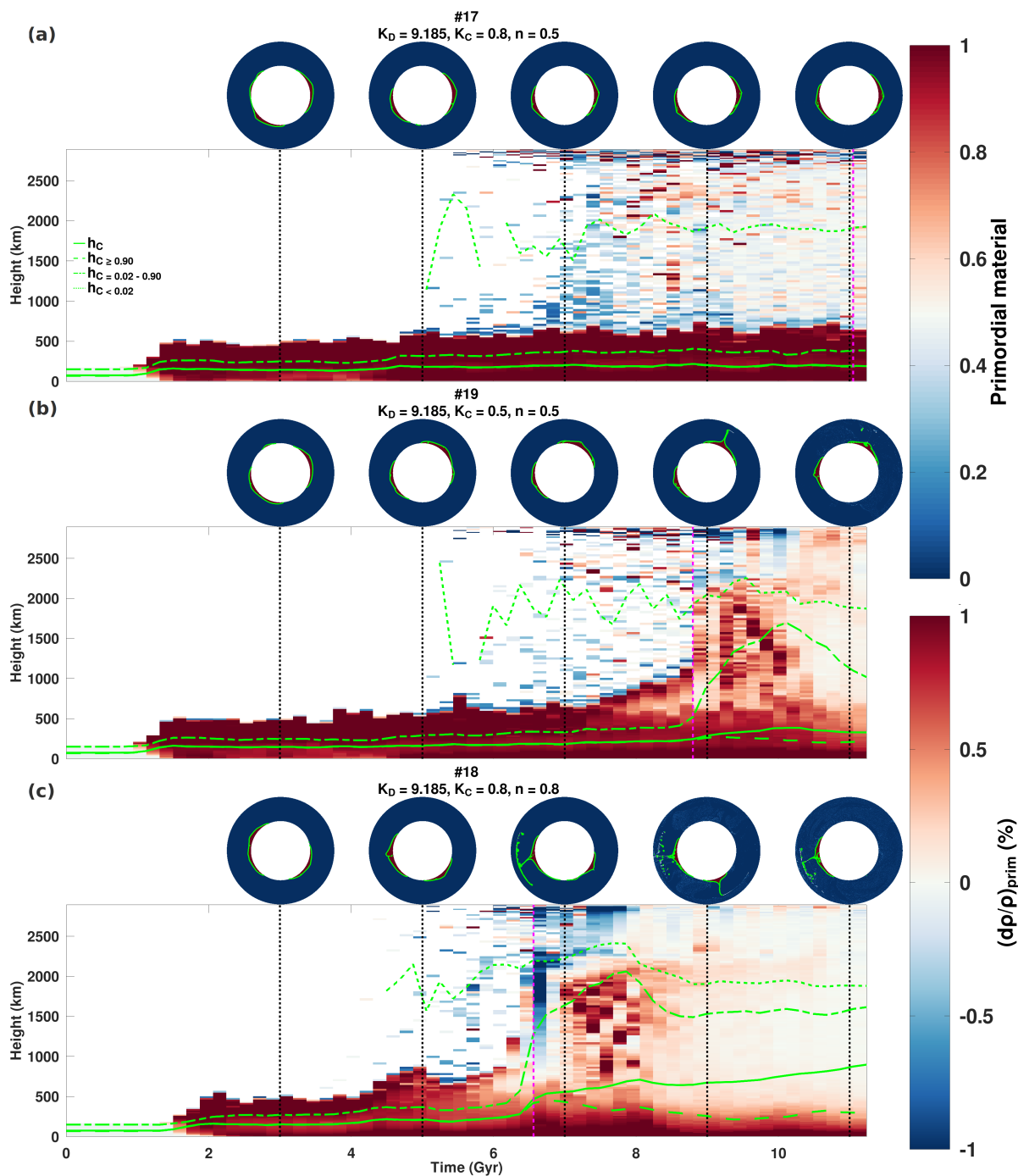
Figure 6. Evolution of the horizontally averaged primordial material density anomalies is illustrated for cases featuring $K_D = 9.185$. Primordial field snapshots are sampled at 2 Gyr intervals starting at 3 Gyr above the timeseries (dashed-black vertical line indicates the time). Mean heights of primordial material are plotted on top of the density anomaly timeseries. The dashed-magenta vertical line indicates the onset of instability in thermochemical reservoirs. Piles are indicated similarly as in Figure 3.

4 Discussion

The evolution of thermochemical reservoirs depends on their temperature and on the mean bottom conductivity. The value of bottom conductivity results mainly from the competing thermal and pressure effects. That is, stronger temperature- dependence (larger n) reduces conductivity, which may or may not compensate (or be exceeded) by depth- dependence (larger K_D).

190 Considering the purely depth- dependent conductivity scenario, heat flow between reservoirs and the surrounding mantle may attain a rate that inhibits reservoir temperature increases due to enrichment in HPEs. That is, a greater lower mantle conductivity stabilizes thermochemical reservoirs by mitigating any (additional) thermal buoyancy imparted by internal heat sources and by increasing heat diffusion in regions where hot instabilities grow. When temperature- dependence (and compositional correction) is considered, the conductivity of reservoirs is reduced with respect to the surrounding mantle. If the depth- conductivity ratio

195 is insufficient to compensate for this conductivity reduction, a negative feedback loop forms whereby a poorly conducting pile cannot rid itself of heat, becomes hotter, and further reduces its conductivity. The imparted thermal buoyancy destabilizes the reservoirs and influences CMB coverage configuration, erosion rate, and the onset of entrainment.

The effect of compositional correction on the stability of thermochemical reservoirs is secondary to the thermal effect. For conductivity models with near-unity top-to-bottom conductivity ratio (when thermal and depth- dependent effects are

200 balanced), greater compositional correction may quicken the onset of instability (e.g., by less than 1 Gyr, comparing cases #12 and #13; Figure S6). When depth- dependence is greater, a greater top-to-bottom conductivity ratio is implied which acts to stabilize the piles. However, the amplitude of conductivity variations is also increased. Thus, a greater compositional correction may quicken the onset of instability (e.g., by approximately 2 Gyr, comparing cases #17 and #19; Figure 6) but take a longer period of time to manifest (e.g., by approximately 4 Gyr, comparing cases #13 and #19).

205 Variations in the physical properties of thermochemical reservoirs, most notably the buoyancy ratio and enrichment in HPEs, have an influence on their long-term evolution. Constraints on these properties are still being determined and subjects of ongoing research. Given the scope of this study, isolating the effect of conductivity on stability may be masked by their first order influences. For example, greater compositional correction for conductivity is related to pile's enrichment in iron and thus implies density increase requiring an increase in buoyancy ratio. In contrast, amount of enrichment in HPEs will directly

210 influence the thermal buoyancy and destabilize piles in the long-term. Furthermore, we do not consider a decaying rate of internal heating. Assuming a mean 3 Gyr half life, internal heating rate should be reduced by almost an order of magnitude by the end of the simulation period we consider. It may be possible that the stronger influence of thermal buoyancy is limited to earlier periods of maximum heat input. The influence of these parameters in conjunction with the moderate heterogeneous conductivity profile we propose (i.e., #17) should be examined in further detail.

215 The core-mantle boundary temperature may also be an important factor in the stability and evolution of thermochemical reservoirs when a heterogeneous conductivity is considered. In our study, the reference state imposes a CMB temperature ($T_{CMB} = 3440$ K) that is on the lower end of the estimates (e.g., Lay et al., 2008; Mosca et al., 2012; Nomura et al., 2014). Boehler (2000); Price et al. (2004) and Kawai & Tsuchiya (2009) suggest greater temperatures in excess of 3750 K and up to 4000 K are possible. For the constant system heating conditions we consider, a greater CMB temperature implies that the

220 mean temperatures in the lowermost mantle will also be increased, resulting in a lower thermal conductivity in that region and within the piles. In addition, higher thermal gradients at the base of the mantle will result in an increase in mean CMB heat flow. Thus, at very high CMB temperatures piles may become unstable. However, stable piles (under hotter conditions) can be accommodated by considering a lower n or a greater depth- dependent conductivity, or by other physical parameters (e.g., temperature- dependence of viscosity, or buoyancy ratio). Therefore, conclusions drawn from our results should be unchanged.

225 Because a cooling bottom boundary is not considered, it is possible that piles evolving with our CMB temperature (or in hotter systems) could become more stable as the mantle cools and the mean lowermost mantle conductivity (and potentially the CMB heat flow) rises. However, examining evolving system heating conditions is out of the scope of our study.

Alternative formulations of the lattice conductivity exist in the literature featuring temperature and density dependences (e.g., Manthilake et al., 2011; Okuda et al., 2017). Furthermore, measurements of the temperature dependent exponent for
230 lower mantle materials may take on values that are less than 0.5 (i.e., between 0.2 and 0.47). For the lattice conductivity we consider, a lower exponent (lesser temperature dependence) will promote stability in piles. In addition, the radiative component of conductivity is much less than the lattice component for temperatures less than the CMB temperature (e.g., Dubuffet et al., 1999). It may be possible that the piles' temperature increases we observe could curb the conductivity reduction due to the lattice component. We do not rule out these possibilities but propose that different conductivity formulations are subjects for
235 future studies.

5 Conclusions

In this study, we investigate the influence of variations in thermal conductivity on thermochemical convection, and find that a heterogeneous conductivity strongly influences the long-term evolution of thermochemical reservoirs. The combined influences of temperature- and depth- variations determines the mean conductivity ratio from top-to-bottom. In the calculations we
240 present, for the mean conductivity profile to be comparable to the conductivity often assumed in numerical models, the depth-dependent ratio must be at least 9 times the surface conductivity. The compositional correction for conductivity only plays a minor role that augments and behaves similarly to conductivity reduction due to temperature. Nevertheless, this effect may be amplified when depth- dependence is increased. For the cases we examine, when the mean conductivity in the lowermost mantle is much greater than the surface conductivity, large reservoirs can be maintained until the end of the simulation.

245

Code and data availability. The numerical code is available by reasonable request to Paul James Tackley. The data corresponding to the numerical simulations are too large to be stored online, but they can be requested from the corresponding authors as well as the input files used to run the simulations.

Author contributions. Joshua M. Guerrero: contributed to the study design, formal analysis, visualization, and writing - original draft prepa-
250 ration. Frédéric Deschamps: contributed to the study design, investigation, visualization, writing - review & editing. Yang Li: contributed to
writing - review & editing. Wen-Pin Hsieh: contributed to consultation on the thermal conductivity model and writing - review & editing.
Paul J. Tackley: contributed to software by designing the 3D thermochemical convection code and writing - review & editing. All authors
collaborated and contributed intellectually to this paper.

Competing interests. The authors declare that they have no conflict of interest.

255 *Acknowledgements.* This study was funded by Ministry of Science and Technology, Taiwan (MoST) grant MOST 110-2116-M-001-025.

References

Boehler, R. 2000. High-pressure experiments and the phase diagram of lower mantle and core materials. Reviews of Geophysics, 38(2), 221-245.

Chang, Y. Y., Hsieh, W. P., Tan, E., & Chen, J. 2017. Hydration-reduced lattice thermal conductivity of olivine in Earth's upper mantle. Proceedings of the National academy of Sciences, 114(16), 4078-4081.

Citron, R. I., Lourenço, D. L., Wilson, A. J., Grima, A. G., Wipperfurth, S. A., Rudolph, M. L., ... & Montési, L. G. (2020). Effects of Heat-Producing Elements on the Stability of Deep Mantle Thermochemical Piles. Geochemistry, Geophysics, Geosystems, 21(4), e2019GC008895.

Davies, D. R., Goes, S., Davies, J. H., Schuberth, B. S. A., Bunge, H. P., & Ritsema, J. (2012). Reconciling dynamic and seismic models of Earth's lower mantle: The dominant role of thermal heterogeneity. Earth and Planetary Science Letters, 353, 253-269.

Deschamps, F., & Hsieh, W. P. 2019. Lowermost mantle thermal conductivity constrained from experimental data and tomographic models. Geophysical Journal International, 219(Supplement 1), S115-S136.

Deschamps, F., Kaminski, E., & Tackley, P. J. 2011. A deep mantle origin for the primitive signature of ocean island basalt. Nature Geoscience, 4(12), 879-882.

Dubuffet, F., & Yuen, D. A. 2000. A thick pipe-like heat-transfer mechanism in the mantle: Nonlinear coupling between 3-D convection and variable thermal conductivity. Geophysical research letters, 27(1), 17-20.

Dubuffet, F., Yuen, D. A., & Rabinowicz, M. 1999. Effects of a realistic mantle thermal conductivity on the patterns of 3-D convection. Earth and Planetary Science Letters, 171(3), 401-409.

Dubuffet, F., Yuen, D. A., & Yanagawa, T. 2000. Feedback effects of variable thermal conductivity on the cold downwellings in high Rayleigh number convection. Geophysical Research Letters, 27(18), 2981-2984.

Garnero, E. J., McNamara, A. K., & Shim, S. H. 2016. Continent-sized anomalous zones with low seismic velocity at the base of Earth's mantle. Nature Geoscience, 9(7), 481-489.

Geballe, Z. M., Sime, N., Badro, J., van Keken, P. E., & Goncharov, A. F. 2020. Thermal conductivity near the bottom of the Earth's lower mantle: Measurements of pyrolite up to 120 GPa and 2500 K. Earth and Planetary Science Letters, 536, 116161.

Gülcher, A. J., Gebhardt, D. J., Ballmer, M. D., & Tackley, P. J. 2020. Variable dynamic styles of primordial heterogeneity preservation in the Earth's lower mantle. Earth and Planetary Science Letters, 536, 116160.

Hernlund, J. W., & Tackley, P. J. 2008. Modeling mantle convection in the spherical annulus. Physics of the Earth and Planetary Interiors, 171(1-4), 48-54.

Heyn, B. H., Conrad, C. P., & Trønnes, R. G. 2020. How thermochemical piles can (periodically) generate plumes at their edges. Journal of Geophysical Research: Solid Earth, 125(6), e2019JB018726.

Hofmeister, A. M. 1999. Mantle values of thermal conductivity and the geotherm from phonon lifetimes. Science, 283(5408), 1699-1706.

Hsieh, W. P., Deschamps, F., Okuchi, T., & Lin, J. F. 2017. Reduced lattice thermal conductivity of Fe-bearing bridgmanite in Earth's deep mantle. Journal of Geophysical Research: Solid Earth, 122(7), 4900-4917.

Hsieh, W. P., Deschamps, F., Okuchi, T., & Lin, J. F. 2018. Effects of iron on the lattice thermal conductivity of Earth's deep mantle and implications for mantle dynamics. Proceedings of the National Academy of Sciences, 115(16), 4099-4104.

Kawai, K., & Tsuchiya, T. 2009. Temperature profile in the lowermost mantle from seismological and mineral physics joint modeling. Proceedings of the National Academy of Sciences, 106(52), 22119-22123.

Klemens, P. G. 1960. Thermal resistance due to point defects at high temperatures. Physical review, 119(2), 507.

Lay, T., Hernlund, J., & Buffett, B. A. 2008. Core–mantle boundary heat flow. Nature geoscience, 1(1), 25-32.

295   Li, Y., Deschamps, F., & Tackley, P. J. 2014. The stability and structure of primordial reservoirs in the lower mantle: insights from models of thermochemical convection in three-dimensional spherical geometry. Geophysical Journal International, 199(2), 914-930.

Li, Y., Vilella, K., Deschamps, F., Zhao, L., & J. Tackley, P. 2018. Effects of iron spin transition on the structure and stability of large primordial reservoirs in Earth's lower mantle. Geophysical Research Letters, 45(12), 5918-5928.

Li, Y., Deschamps, F., Yang, J., Chen, L., Zhao, L., & Tackley, P. J. 2019. Effects of the Compositional Viscosity Ratio on the Long-Term

300   Evolution of Thermochemical Reservoirs in the Deep Mantle. Geophysical Research Letters, 46(16), 9591-9601.

Li, Y., Deschamps, F., Shi, Z., Guerrero J. M., Hsieh, W. P., & Tackley, P. J. 2022 Influence of composition-dependent thermal conductivity on the long-term evolution of primordial reservoirs in Earth's lower mantle. Earth Planets Space 74, 46 (2022). https://doi.org/10.1186/s40623-022-01608-3

Manthilake, G. M., de Koker, N., Frost, D. J., & McCammon, C. A. 2011. Lattice thermal conductivity of lower mantle minerals and heat

305   flux from Earth's core. Proceedings of the National Academy of Sciences, 108(44), 17901-17904.

Marzotto, E., Hsieh, W. P., Ishii, T., Chao, K. H., Golabek, G. J., Thielmann, M., & Ohtani, E. 2020. Effect of water on lattice thermal conductivity of ringwoodite and its implications for the thermal evolution of descending slabs. Geophysical Research Letters, 47(13), e2020GL087607.

Mosca, I., Cobden, L., Deuss, A., Ritsema, J., & Trampert, J. 2012. Seismic and mineralogical structures of the lower mantle from proba-

310   bilistic tomography. Journal of Geophysical Research: Solid Earth, 117(B6).

Nomura, R., Hirose, K., Uesugi, K., Ohishi, Y., Tsuchiyama, A., Miyake, A., & Ueno, Y. 2014. Low core-mantle boundary temperature inferred from the solidus of pyrolite. Science, 343(6170), 522-525.

Okuda, Y., Ohta, K., Yagi, T., Sinmyo, R., Wakamatsu, T., Hirose, K., & Ohishi, Y. 2017. The effect of iron and aluminum incorporation on lattice thermal conductivity of bridgmanite at the Earth's lower mantle. Earth and Planetary Science Letters, 474, 25-31.

315   Price, G. D., Alfè, D., Vočadlo, L., & Gillan, M. J. 2004. The Earth's core: an approach from first principles. American Geophysical Union.

Tackley, P. J. 1998. Three-dimensional simulations of mantle convection with a thermo-chemical basal boundary layer: D. The Core-Mantle Boundary Region, Geodyn. Ser, 28, 231-253.

Tackley, P. J. 2008. Modelling compressible mantle convection with large viscosity contrasts in a three-dimensional spherical shell using the yin-yang grid. Physics of the Earth and Planetary Interiors, 171(1), 7-18.

320   Tan, E., Leng, W., Zhong, S., & Gurnis, M. 2011. On the location of plumes and lateral movement of thermochemical structures with high bulk modulus in the 3-D compressible mantle. Geochemistry, Geophysics, Geosystems, 12(7).

Tosi, N., Yuen, D. A., de Koker, N., & Wentzcovitch, R. M. 2013. Mantle dynamics with pressure-and temperature-dependent thermal expansivity and conductivity. Physics of the Earth and Planetary Interiors, 217, 48-58.

Trampert, J., Deschamps, F., Resovsky, J., & Yuen, D. 2004. Probabilistic tomography maps chemical heterogeneities throughout the lower

325   mantle. Science, 306(5697), 853-856.

Xu, Y., Shankland, T. J., Linhardt, S., Rubie, D. C., Langenhorst, F., & Klasinski, K. 2004. Thermal diffusivity and conductivity of olivine, wadsleyite and ringwoodite to 20 GPa and 1373 K. Physics of the Earth and Planetary Interiors, 143, 321-336.

Yanagawa, T. K., Nakada, M., & Yuen, D. A. 2005. Influence of lattice thermal conductivity on thermal convection with strongly temperature-dependent viscosity. Earth, planets and space, 57(1), 15-28.